

Something something something physics

Steven Green
of Emmanuel College

A dissertation submitted to the University of Cambridge
for the degree of Doctor of Philosophy

Abstract

LHCb is a b-physics detector experiment which will take data at the 14 TeV LHC accelerator at CERN from 2007 onward...

Declaration

This dissertation is the result of my own work, except where explicit reference is made to the work of others, and has not been submitted for another qualification to this or any other university. This dissertation does not exceed the word limit for the respective Degree Committee.

Andy Buckley

Acknowledgements

Of the many people who deserve thanks, some are particularly prominent, such as my supervisor...

Preface

This thesis describes my research on various aspects of the LHCb particle physics program, centred around the LHCb detector and LHC accelerator at CERN in Geneva.

For this example, I'll just mention Chapter ?? and Chapter ??.

Contents

| | |
|--|-----------|
| 1. The Sensitivity of CLIC to Anomalous Gauge Couplings through Vector Boson Scattering | 1 |
| 1.1. Background | 1 |
| 1.2. Event Generation | 2 |
| 1.3. Simulation and Reconstruction | 5 |
| 1.4. Validation of New Samples | 6 |
| 1.5. Analysis Processor and Jet Pairing | 6 |
| 1.6. Methodology for Fitting | 11 |
| 1.7. Optimisation of Jet Reconstruction | 14 |
| 1.8. Event Selection | 17 |
| 1.8.1. Pre Selection - 1.4 TeV | 19 |
| 1.8.2. MVA - 1.4 TeV | 22 |
| 1.8.3. Pre Selection - 3 TeV | 24 |
| 1.8.4. MVA - 3 TeV | 24 |
| 1.9. Fit | 24 |
| A. Pointless extras | 27 |
| A.1. Anomalous Gauge Coupling Quartic Vertices Of Relevance in Vector Boson Scattering | 27 |
| A.2. χ^2 Contour Plots for Jet Algorithm Optimisation | 30 |
| Bibliography | 37 |
| List of figures | 39 |
| List of tables | 41 |

*“Writing in English is the most ingenious torture
ever devised for sins committed in previous lives.”*

— James Joyce

Chapter 1.

The Sensitivity of CLIC to Anomalous Gauge Couplings through Vector Boson Scattering

“Kids, you tried your best, and you failed miserably. The lesson is, never try.”

— Homer Simpson

1.1. Background

A process that will show sensitivity to the α_4 and α_5 anomalous gauge couplings in the CLIC experiment is vector boson scattering. There are several channels that will be affected by these anomalous couplings at CLIC and these are summarised in figures ??, ??, reffig:vbswz and ?? where $q = u, d, s, b, c$ and $l = e, \mu, \tau, \nu_e, \nu_\mu, \nu_\tau$.

To determine whether an event is sensitive to α_4 and α_5 it will be necessary to determine whether the visible final states have been produced from the decay of W and Z bosons. A key discriminator in this procedure will be the invariant mass of the W and Z candidates. In light of this the hadronic decays of the W and Z bosons are only considered as the leptonic decays may contain neutrinos.

As the W and Z bosons in vector boson scattering are intermediate states in the Feynman diagrams, they will not be directly observed in the detector and will instead

contribute to processes with the final states containing possible decay products of the bosons $\nu\nu qqqq$, $l\nu qqqq$ and $ll qqqq$. In theory all processes will be affected by non zero α_4 and α_5 , however, the effects may be extremely small as they contribute to very high order expansions of the Hamiltonian. Event generation software does not calculate the expansions of the Hamiltonian to all orders, but instead truncates the expansion to leave the dominant terms. In the case of anomalous couplings this corresponds to certain final state cross sections being invariant to changes in α_4 and α_5 .

1.2. Event Generation

The event generation software used by the CLIC experiment is Whizard [7, 11]. Whizard version 1.97 was used for generating the new samples, while version 1.95 is used for the official CLIC samples. It was recommended by the Whizard authors to use version 1.97 as it contains a unitarisation scheme that ensures the probabilities remain physical up to high energies when considering the effect of anomalous gauge couplings.

It was necessary to specify the anomalous coupling model in Whizard to study their impact, however, this did enforce a unit CKM matrix. In the context of vector boson scattering this will restrict the decays of the W to $d\bar{u}$ and $s\bar{c}$, the W^+ to $u\bar{d}$ and $c\bar{s}$ and the Z to $u\bar{u}$, $d\bar{d}$, $s\bar{s}$, $c\bar{c}$, $b\bar{b}$. This has little overall impact on the study as the cross section calculation using this model was, within the errors quoted by Whizard, identical to the standard model CKM matrix. The only aspect of the analysis effected by this modification is flavour tagging of jets and this will be addressed in subsequent chapters.

To find out which states show sensitivity to the anomalous couplings cross section calculations were made using different values of α_4 and α_5 for relevant processes involving the hadronic decays of the W and Z bosons from vector boson scattering. These results can be found in table 1.1 for 1.4 TeV samples and 1.2 for 3 TeV samples. The only final states showing sensitivity to the anomalous couplings are $\nu\nu qqqq$, $l\nu qqqq$ and $ll qqqq$, which correspond to the final states from the Feynman diagrams shown above in figures ??, ??, reffig:vbswz and ??. As this analysis focuses on the hadronic decays of the bosons involved in vector boson scattering the final states involving leptonic decays of the bosons e.g. $\nu\nu llqq$ were not included in this cross check. These leptonic dominated final states were also removed from the background

samples used in this study as isolated lepton finding would largely veto all such events from selection.

This cross check was also applied to the background samples that are to be included in this analysis. It was found that the cross sections was invariant to changes in α_4 and α_5 for the following processes:

- $e^+e^- \rightarrow qqqq$
- $e^+e^- \rightarrow \nu\nu qq$
- $e^+e^- \rightarrow l\nu qq$
- $e^+e^- \rightarrow llqq$
- $e^+e^- \rightarrow qq$
- $\gamma_{\text{EPA}}e^- \rightarrow qqqqe^-$
- $\gamma_{\text{BS}}e^- \rightarrow qqqqe^-$
- $e^+\gamma_{\text{EPA}} \rightarrow qqqqe^+$
- $e^+\gamma_{\text{BS}} \rightarrow qqqqe^+$
- $\gamma_{\text{EPA}}e^- \rightarrow qqqq\nu$
- $\gamma_{\text{BS}}e^- \rightarrow qqqq\nu$
- $e^+\gamma_{\text{EPA}} \rightarrow qqqq\nu$
- $e^+\gamma_{\text{BS}} \rightarrow qqqq\nu$
- $\gamma_{\text{EPA}}\gamma_{\text{EPA}} \rightarrow qqqq$
- $\gamma_{\text{EPA}}\gamma_{\text{BS}} \rightarrow qqqq$
- $\gamma_{\text{BS}}\gamma_{\text{EPA}} \rightarrow qqqq$
- $\gamma_{\text{BS}}\gamma_{\text{BS}} \rightarrow qqqq$

The sensitivity of an individual event to the anomalous gauge couplings is determined through an event weight. This weight corresponds to the ratio using non-zero α_4 and α_5 and using zero α_4 and α_5 of the square of the matrix element used in the cross section calculation. This reweighting procedure has many advantages over the alternative procedure of generating new samples with fixed α_4 and α_5 most notably

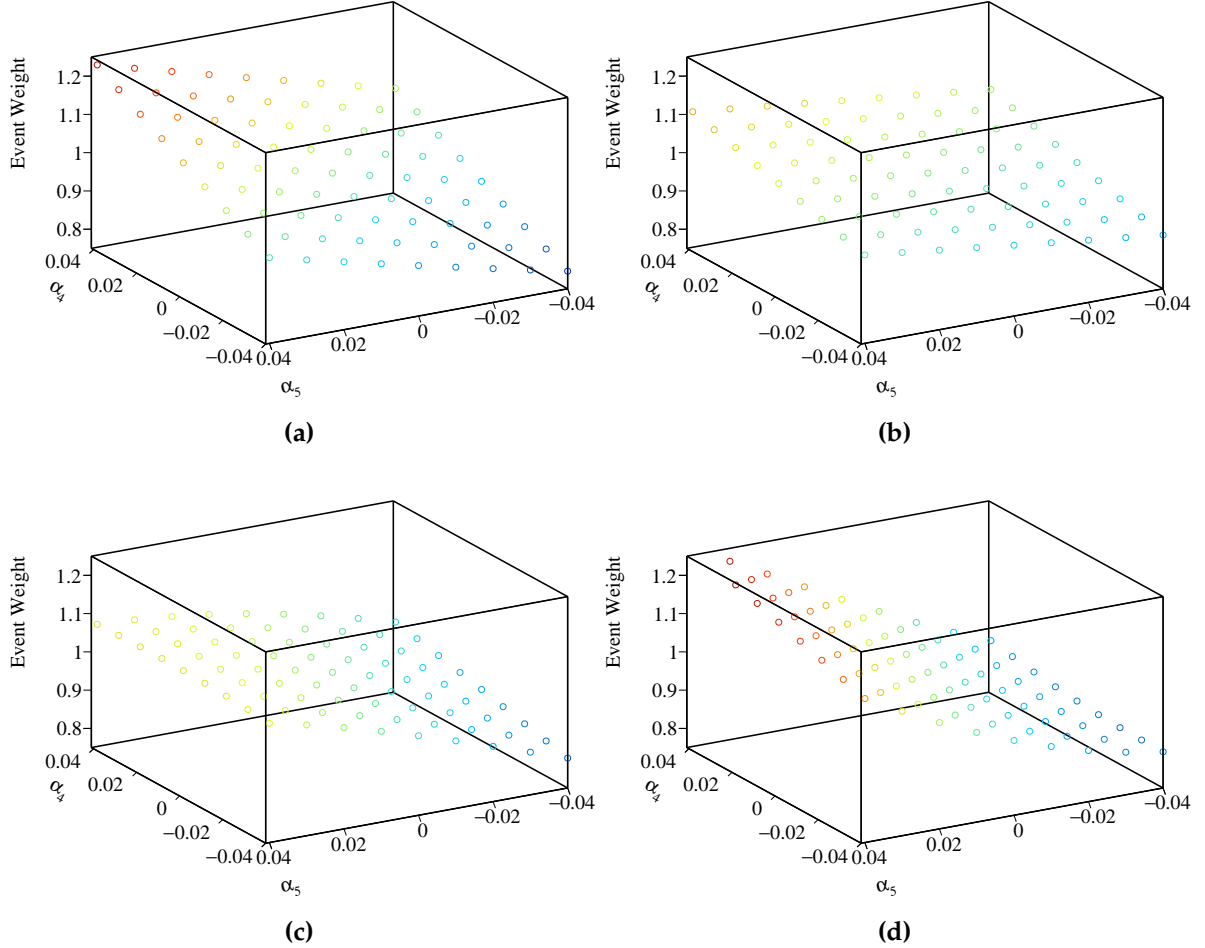


Figure 1.1.: A selection of plots showing how the event weight changes when varying the anomalous couplings α_4 and α_5 for 1.4TeV $\nu\nu qqqq$ final state events.

the absence of systematic errors that may appear in new event generation. Each event picks up different weights based on α_4 and α_5 as the matrix element contributions from the anomalous couplings depend upon the kinematics of the final state, which is unique for each event. Examples of the event weights as a function of α_4 and α_5 for selected events is shown in figure 1.3.

The cross check shows that the most sensitive channel to the anomalous gauge couplings is the $\nu\nu qqqq$ indicating that the best sensitivity measurement should focus upon this channel, which is the aim of this analysis.

The CLIC experiment has a repository of simulated and reconstructed samples that can be used for physics analyses, however, for the relevant final states there is no way to calculate the event weights for these samples. Therefore, new samples

for which reweighting is possible were created and processed through the CLIC reconstruction chain. New samples were created only for the $\nu\nu qqqq$ final state as the $l\nu qqqq$ and $ll qqqq$ final states have a significantly lower sensitivity. As will be shown in subsequent chapters, the application of an isolated lepton finder in the selection processor will largely veto the $l\nu qqqq$ and $ll qqqq$ final states, therefore, the absence of weight information for these final states will not significantly affect the sensitivity measurement based on the $\nu\nu qqqq$ final state.

| Final State | Cross Section [fb] ($\alpha_4 = \alpha_5 = 0.00$) | Cross Section [fb] ($\alpha_4 = \alpha_5 = 0.05$) | Percentage Change[%] | CLIC Cross Section [fb] |
|----------------------------------|--|--|-------------------------|----------------------------|
| $e^+e^- \rightarrow \nu\nu qqqq$ | 20.8 | 34.6 | +66.3 | 24.7 |
| $e^+e^- \rightarrow l\nu qqqq$ | 112 | 113 | +0.9 | 115.3 |
| $e^+e^- \rightarrow ll qqqq$ | 59.7 | 68.6 | +14.9 | 62.1 |

Table 1.1.: Cross section for selected processes for given value of α_4 and α_5 at 1.4 TeV.

| Final State | Cross Section [fb] ($\alpha_4 = \alpha_5 = 0.000$) | Cross Section [fb] ($\alpha_4 = \alpha_5 = 0.005$) | Percentage Change[%] | CLIC Cross Section [fb] |
|----------------------------------|---|---|-------------------------|----------------------------|
| $e^+e^- \rightarrow \nu\nu qqqq$ | 51.2 | 77.7 | +51.8 | 71.5 |
| $e^+e^- \rightarrow l\nu qqqq$ | 111.9 | 115.9 | +3.6 | 106.6 |
| $e^+e^- \rightarrow ll qqqq$ | 169.7 | 161.7 | -4.9 | 169.3 |

Table 1.2.: Cross section for selected processes for given value of α_4 and α_5 at 3 TeV.

1.3. Simulation and Reconstruction

The CLID_ILD detector [1] was simulated using MOKKA [10], a GEANT4 [2] wrapper providing detailed geometric descriptions of detector concepts for the linear collider. Events were reconstructed using MARLIN [5] a c++ framework designed for reconstruction at the linear collider. PandoraPFA [9, 13] is used to apply particle flow calorimetry to these samples and to produce PFOs that are used in this analysis.

Using the CLIC_ILD detector for this analysis provides access to the background samples created by the CLIC collaboration. The CLIC_ILD detector has a 60 layer scintillator-tugsten HCal in comparison to the 48 layer HCal found in the default ILD detector. The increase in thickness of the detector for the CLIC experiment is

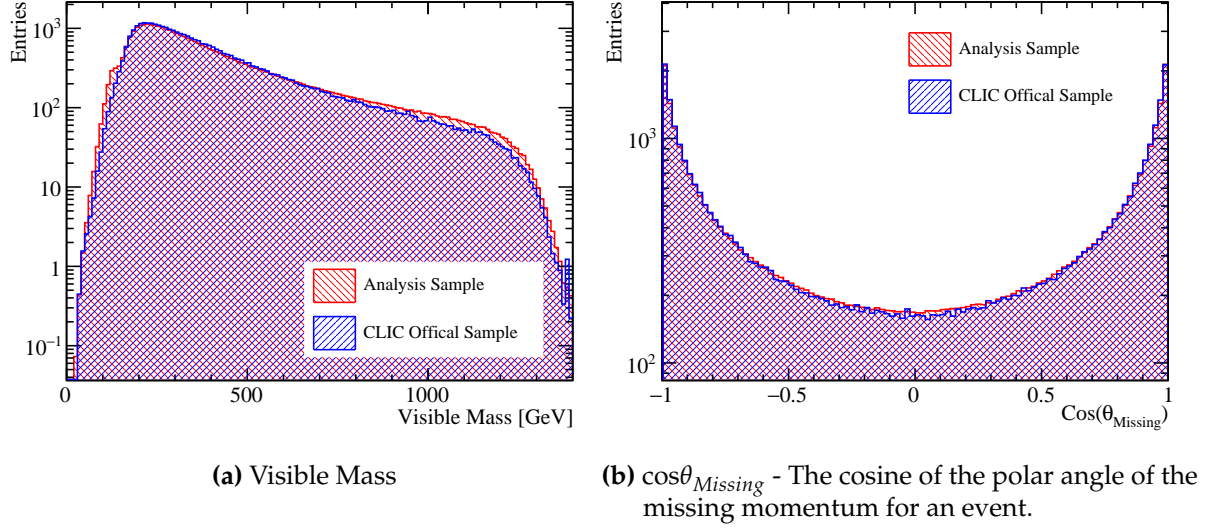


Figure 1.2.: Comparison of various distributions between samples used in this analysis and the official CLIC samples for the $\nu\nu qq qq$ final state.

needed to compensate for the effects of leakage at the higher energies seen by the CLIC experiment in comparison to the ILC. Practically speaking the ILD and CLIC_ILD detectors are otherwise identical.

1.4. Validation of New Samples

An identical setup to that used for the official CLIC sample was used for the event generation and reconstruction. Several reconstructed level distributions were compared to the official CLIC samples and all were found to be comparably to each other. A selection of these distributions is shown in figure 1.2.

1.5. Analysis Processor and Jet Pairing

For both signal and background events the MarlinFastJet processor, a wrapper for the FastJet [4] process, is used to cluster the events into 4 jets. These are jets assumed to be from the hadronic decays of the bosons involved in the vector scattering process. These jets are paired up such that on the assumption that the correct pair arises when the invariant masses of the two pairs are closest together. The longitudinally invariant

kt jet algorithm in exclusive modes is used for the jet clustering. This jet algorithm proceeds as follows:

- For each pair of particles i and j work out the kt distance and beam distance $d_{iB} = p_t^2$.

$$d_{ij} = \min(p_{ti}^2, p_{tj}^2) \Delta R_{ij}^2 / R^2 \quad (1.1)$$

where $\Delta R_{ij}^2 = (y_i - y_j)^2 + (\phi_i - \phi_j)^2$. p_t is the transverse momentum of the particle with respect to the beam axis, y_i is the rapidity of particle i and ϕ_i is the azimuthal angle of particle i . R is a configurable parameter that typically is of the order of 1.

- Find the minimum distance d_{\min} of all the k_t and beam distances. If the minima occurs for a k_t distance, merge particles i and j , summing their 4-momenta in the energy combination scheme (also configurable). If the beam distance is the minimum declare particle i to be apart of the "beam" jet and remove it from the list of particles and not included in the final output jets.
- Repeat until no particles are left or the requested number of jets have been created (or optionally apply a minimum d_{cut} where clustering stops, but here the event is forced into 4 jets).

An inclusive mode is available, but not applied here as the finally number of jets in the output varies and events need to be clustered into 4 jets for this analysis. Two other clustering modes were considered, but were found to be inappropriate for this analysis as is shown in figure 1.3. They were:

- The kt algorithm for e+e colliders (or Durham algorithm) where $d_{ij} = 2\min(E_i^2, E_j^2)(1 - \cos\theta_{ij})$ and d_{iB} is not used. θ_{ij} is the opening angle of the particles. In the collinear limit this corresponds to the relative transverse momentum of the particles. Unlike the other algorithm choices this is not invariant to boosts along the beam direction as in theory for e+e colliders the collision should occur with no net 3 momentum, unlike hadron colliders where the events have a net 3-momentum. However, the presence of ISR and beam effects makes this algorithm inappropriate for CLIC. The major failure of this algorithm choice is the absence of diB as this associates too many background particles to jets when applied at CLIC.

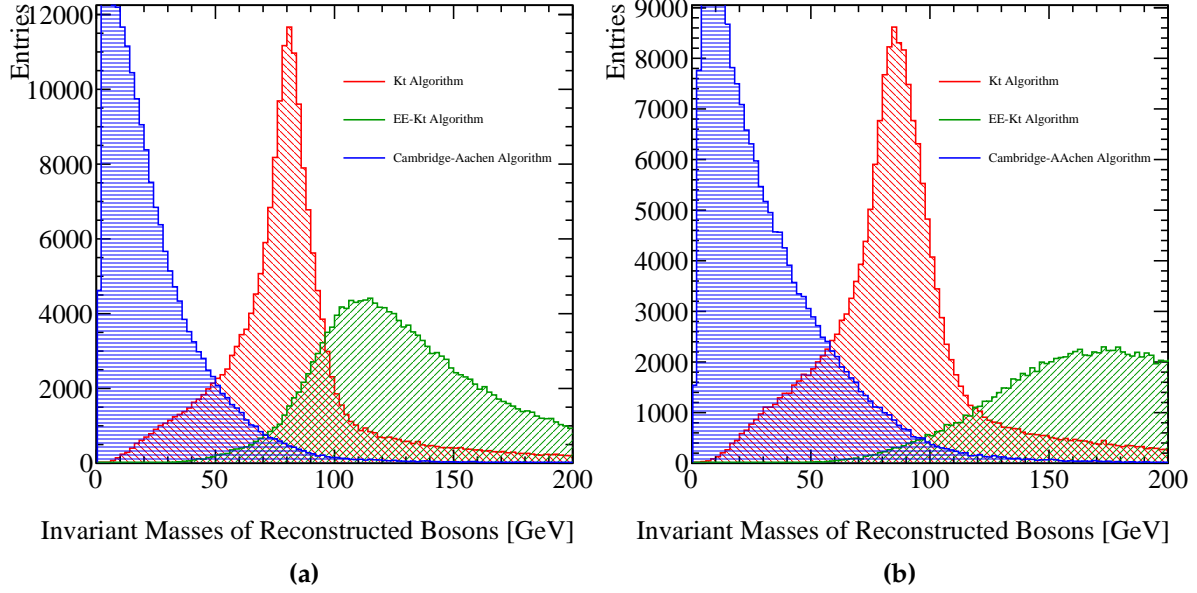


Figure 1.3.: Reconstructed masses for different choices of jet algorithm for 1.4 TeV and 3 TeV $\nu\nu qqqq$ events. These masses arise by forcing the reconstructed events into 4 jets and then pairing up the jets into pairs such that the reconstructed invariant masses of the pairs are closest to each other. These samples should be dominated by vector boson scattering involving pairs of W bosons and so it is expected that a peak at the W boson true mass should be observed. As this does not occur for the Cambridge-Aachen algorithm or the ee_kt algorithm they were deemed unsuitable for this analysis at both 1.4 and 3 TeV. In the case of the kt algorithm and the ee_kt algorithm an R parameter of 0.7 was used.

- The Cambridge/Aachen jet algorithm where $d_{ij} = \Delta R_{ij}^2/R^2$ and $d_{iB} = 1$. This algorithm gave poor performance as it is based entirely on spacial information and does not account for the transverse momentum or energy of the particles being grouped. In essence this is a cone clustering algorithm with a cone radius defined through $\Delta R_{ij} = R$, which even for large R was found to throw away too much energy in the event to be useful for this analysis. This algorithm can be useful for events with small jets that are highly boosted, but in this case the jets are too large to be successfully merged.

An isolated lepton finder is included in the analysis chain in an attempt to reject background events containing leptons. The LCFIPlus [12] processor is also run on these events once clustered into jets to produce a value for the B and C tag likelihood for a jet.

This information is available for background rejection rather than contributing to the sensitivity of the event to the anomalous couplings. The LCFIPlus vertex processor was trained using events of $e^+e^- \rightarrow Z\nu\nu \rightarrow q\bar{q}\nu\nu$ for $q = u, d, s, c, b$.

Finally, an analysis processor is run, which calculates a number of variables used downstream in the analysis. Included in these are:

- Number of PFOs in the jets and the paired up bosons.
- Number of charged PFOs in the jets and paired up bosons.
- Highest energy PFO: energy, momentum, transverse momentum, $\cos\theta$.
- Highest energy electron PFO: energy, momentum, transverse momentum, $\cos\theta$.
- Highest energy muon PFO: energy, momentum, transverse momentum, $\cos\theta$.
- Highest energy photon PFO: energy, momentum, transverse momentum, $\cos\theta$.
- (If in existence) Highest and second highest energy isolated lepton: energy, momentum, transverse momentum, $\cos\theta$.
- Bosons: energy, momentum, transverse momentum, $\cos\theta$.
- Invariant mass of the boson pair.
- Jets: energy, momentum, transverse momentum, $\cos\theta$.
- $\cos\theta$ Of the missing 3-momentum vector.
- Recoil mass.
- Invariant mass of the visible system.
- y_i, y_{i+1} . Jet clustering parameters ranging from $i = 0$ to 6.
- $\cos\theta_{jet}^*$. This is the opening angle of a pair of jets, assumed to be from a single boson, in the rest frame of the boson.
- $\cos\theta_{Boson}^*$. This is the opening angle of a pair of bosons, assumed to be from vector boson scattering, in the rest frame of the di-boson pair.
- Transverse momentum and energy of the event.
- Acolinearity of the jet pairs forming the bosons and the acolinearity of the boson pair.

- Principle thrust T and the thrust axes $\bar{\mathbf{n}}$. Note $\bar{\mathbf{n}}$ is a unit vector. These are defined by the following equation

$$T = \max_{\bar{\mathbf{n}}} \left(\frac{\sum_i \mathbf{p}_i \cdot \bar{\mathbf{n}}}{\sum_i |\mathbf{p}_i|^2} \right) \quad (1.2)$$

- The major and minor thrust values. These are defined with respect to the thrust axes $\bar{\mathbf{n}}$ in the following way:

$$T = \max_{\bar{\mathbf{n}}_{major}} \left(\frac{\sum_i \mathbf{p}_i \cdot \bar{\mathbf{n}}_{major}}{\sum_i |\mathbf{p}_i|^2} \right) \quad (1.3)$$

where $\bar{\mathbf{n}}_{major} \cdot \bar{\mathbf{n}} = 0$. Similarly the minor thrust value is defined as

$$T = \frac{\sum_i \mathbf{p}_i \cdot \bar{\mathbf{n}}_{minor}}{\sum_i |\mathbf{p}_i|^2} \quad (1.4)$$

where $\bar{\mathbf{n}}_{minor} \cdot \bar{\mathbf{n}} = \bar{\mathbf{n}}_{minor} \cdot \bar{\mathbf{n}}_{major} = 0$

- Sphericity. This is defined using the sphericity tensor S^{ab} defined as:

$$S^{ab} = \frac{\sum_i p_i^\alpha p_j^\alpha}{\sum_{i,\alpha=1,2,3} |p_i^\alpha|^2} \quad (1.5)$$

Where p_i are the components of the momenta of particle i in the frame of the detector and the sum runs over all particles in the event. Sphericity is defined as $S = \frac{3}{2}(\lambda_2 + \lambda_3)$, where λ_i are the eigenvalues of the sphericity tensor defined such $\lambda_1 \geq \lambda_2 \geq \lambda_3$. This provides a measure of how spherical the reconstructed event topology is with isotropic events having $S \approx 1$, while two jet events have $S \approx 0$. (Also $\lambda_1 + \lambda_2 + \lambda_3 = 1$.)

- Aplanarity. Aplanarity is defined as $\frac{3}{2}\lambda_3$ where λ_3 is an eigenvalue of the sphericity tensor. This provides a measure of whether an event is linear or planar.
- B and C tag values for the jets, the min and max B and C tag values for the bosons.

Alongside these variables, for the $\nu\nu q\bar{q}q\bar{q}$ final state a number of Monte-Carlo variables are calculated for informative purposes and are not used in the analysis. These include:

- The quark and neutrino 4 momenta.

- Invariant mass of boson pair using MC pairing and MC energy.
- Invariant mass of boson pair using MC pairing and reconstructed jet energy.

1.6. Methodology for Fitting

It is necessary to discuss the fitting procedure in this analysis as the optimisation of the jet algorithms relies on this methodology. In this section only the signal events are considered to determine the underlying sensitivity of the CLIC detector to the anomalous couplings. This decision was made to save analysis of the large number of background samples in the optimisation of the jet reconstruction algorithms, while still optimising the algorithm on the physics of interest.

The sensitivity of CLIC to the anomalous gauge couplings is determined through the use of a χ^2 fit to the distribution of $\cos\theta_{jets}^*$ where θ_{jets}^* is the angle between the two jets produced from the hadronic decay of the W/Z boson in the rest frame of that boson. The distribution of $\cos\theta_{jets}^*$ proved to be sensitive to the anomalous gauge couplings as shown in figure 1.4.

Another distribution considered for the sensitivity study was $\cos\theta_{Bosons}^*$ where θ_{Bosons}^* is the angle between the two bosons produced in vector boson scattering in the rest frame of the boson pair. This distribution was found to be less sensitive to the anomalous gauge couplings than $\cos\theta_{jets}^*$, which can be seen when comparing figures 1.4 and 1.5, and so was not considered for the rest of this study. Furthermore, it was found that a two dimensional χ^2 fit produced by combining $\cos\theta_{jets}^*$ and $\cos\theta_{Bosons}^*$ did not improve the sensitivity significantly in comparison to $\cos\theta_{jets}^*$.

The $\cos\theta_{jets}^*$ variable was binned in histograms of 10 bins before being converted into a value of χ^2 . This binning was selected to maximise the number of bins in the distribution, while minimising the effect of large bin by bin fluctuations arising from individual events with large event weights.

At 1.4 TeV event weights were produced from Whizard stepping along α_4 and α_5 in steps of 0.01 ranging from -0.07 to 0.07 as shown in figure 1.3, however, to produce a smooth χ^2 contour much finer sampling is needed. While it is feasible to generate new event weights in Whizard for any pair of α_4 and α_5 it is time consuming making it impractical for this analysis. To overcome this difficulty bicubic interpolation is

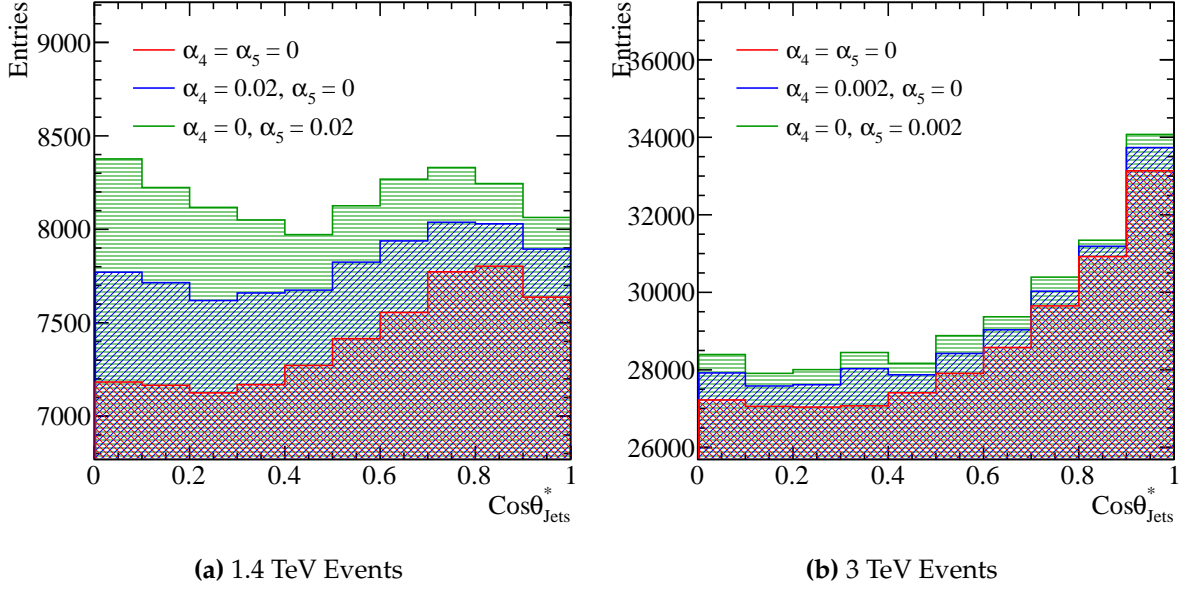


Figure 1.4.: Sensitivity of $\cos\theta_{jets}^*$ to anomalous couplings at 1.4 and 3 TeV. The jet algorithm used for this example was the longitudinally invariant kt algorithm with an R parameter of 0.7. This sample corresponds to pure signal of hadronic decays in vector boson scattering i.e. $\nu\nu qqqq$.

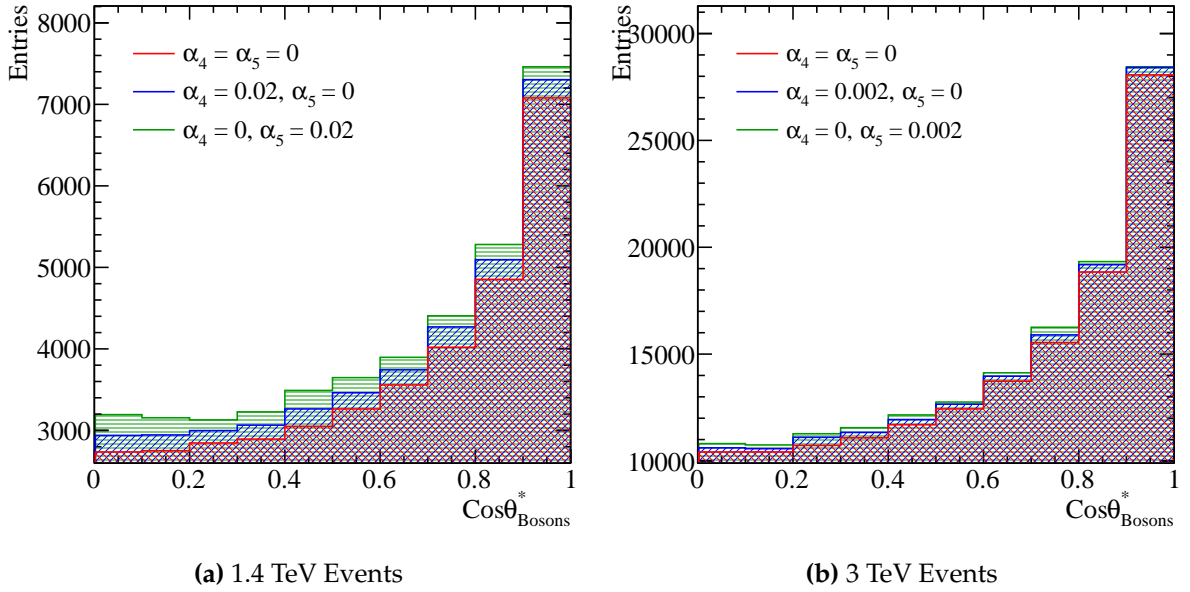


Figure 1.5.: Sensitivity of $\cos\theta_{Bosons}^*$ to anomalous couplings at 1.4 and 3 TeV. The jet algorithm used for this example was the longitudinally invariant kt algorithm with an R parameter of 0.7. This sample corresponds to pure signal of hadronic decays in vector boson scattering i.e. $\nu\nu qqqq$.

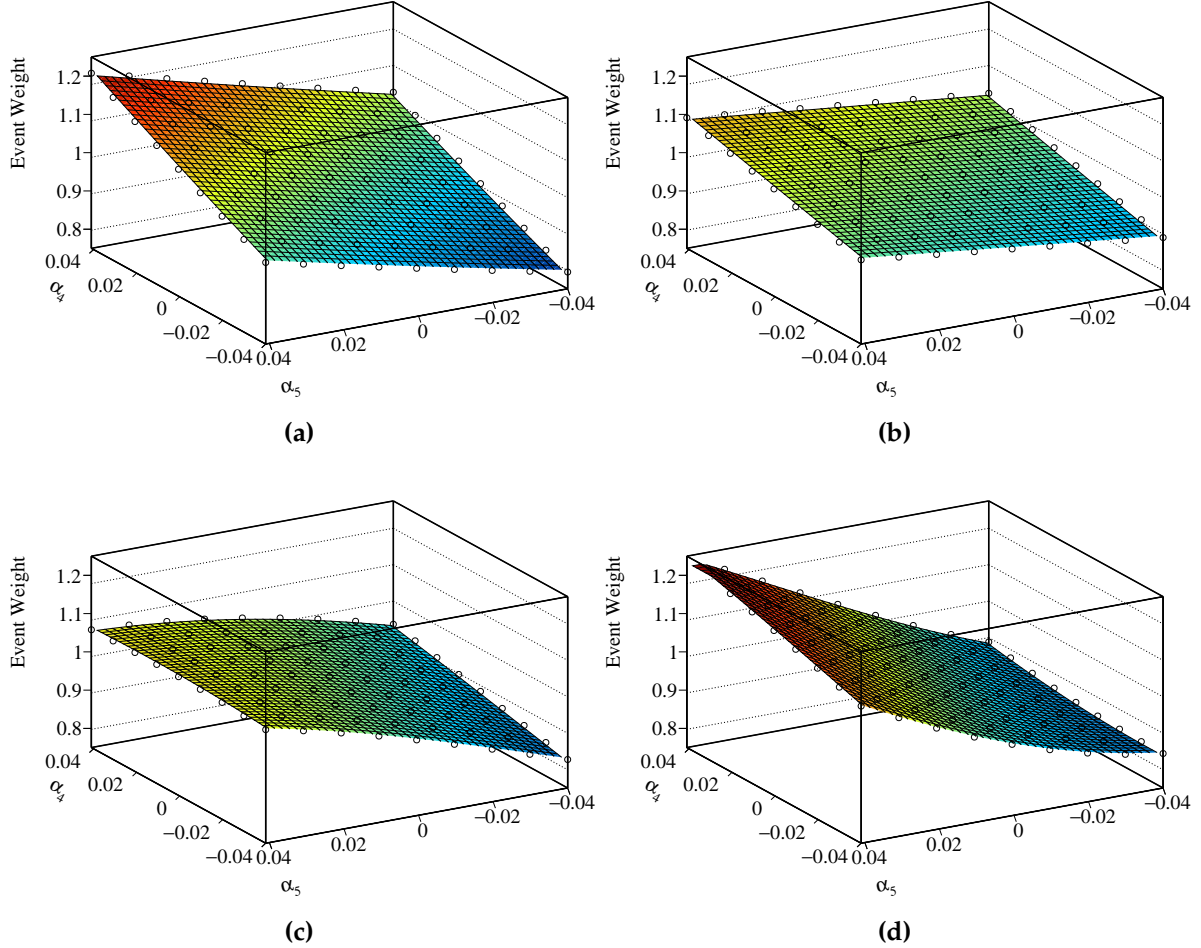


Figure 1.6.: A selection of plots showing how the event weight changes when varying the anomalous couplings α_4 and α_5 for 1.4TeV $\nu\nu qqqq$ final state events. The hollow circles show the event weight produced from the generator while the surface shown is found using bicubic interpolation between those points.

applied between these points to allow for the extract of event weights anywhere within the range -0.05 to 0.05. As figure 1.6 shows the interpolated surface proves to be a good fit to the data produced from the generator in that it is smooth and continuous.

Similarly at 3 TeV the same procedure was used but stepping occurs in steps of 0.001 ranging from -0.007 to 0.007 in both α_4 and α_5 . These ranges proved to be sufficient for the contours of interest for the CLIC sensitivity analysis at this energy.

Using these interpolated surfaces for the event weights, distribution of $\cos\theta_{jets}^*$ were produced stepping across α_4 and α_5 in steps of 0.0001 at 1.4 TeV and 0.00001 at 3 TeV. Each distribution was converted into a value of χ^2 using the following formula:

$$\chi^2 = \sum_i \frac{(O_i - E_i)^2}{E_i} \quad (1.6)$$

where O_i is the observed bin content for bin i in the distribution with non-zero α_4 and α_5 and E_i is the expected bin content for bin i in the distribution with zero α_4 and α_5 i.e. the standard model expected value.

1.7. Optimisation of Jet Reconstruction

The jet algorithm used for this analysis is the longitudinally invariant k_t algorithm as described in section 1.5. The parameter choices under consideration for optimisation are the R parameter, used in the k_t algorithm definition, used and the PFO selection.

A number of cuts [9] are applied to the transverse momenta and the time of the PFOs produced by PandoraPFA to reduce the PFOs into a subset that are believed to originate from the desired interaction in an attempt to veto the overlaid $\gamma\gamma \rightarrow \text{Hadron}$ background events. Different options for these cuts give rise to the tight, default and loose selected PFOs that are considered in this optimisation.

The optimal sensitivity is achieved for either loose selected PFOs with an R parameter of 0.7 or default selected PFOs with an R parameter of 0.9 as can be seen from tables 1.3 and 1.4. As a tie breaker between these options the separation power, the fraction of events misidentified as either arising from a WW pair or a ZZ pair, was considered. Again performance was similar, but there was a slight preference towards the use of selected PFOs and an R parameter of 0.9. While not used in the primary analysis the separation of samples into WW and ZZ events is important for an extension analysis found in section BLAH.

The optimal contours can be found in figure 1.7 and the optimal 1D plot used to produce the errors references in the tables 1.3 and 1.4 can be found in figures 1.8 and 1.9 respectively. All other contours and plots for this optimisation can be found in the appendices.

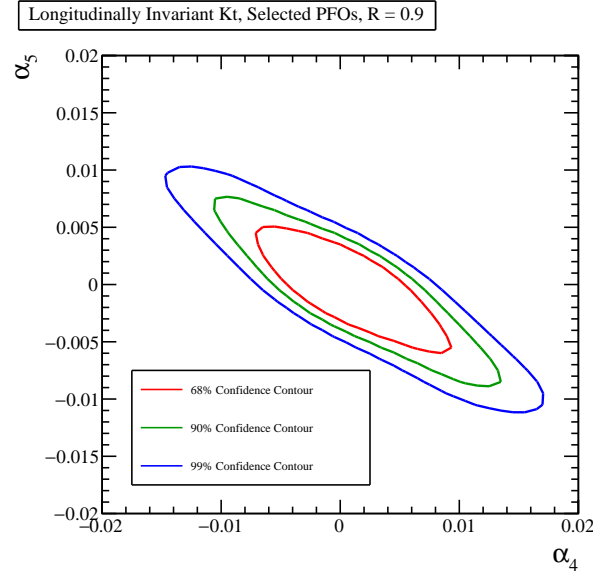


Figure 1.7.: χ^2 Sensitivity contours for the $qqqq\nu\nu$ final state arising from a fit to $\cos\theta_{\text{jets}}^*$ at 1.4 TeV for the optimal jet reconstruction parameters.

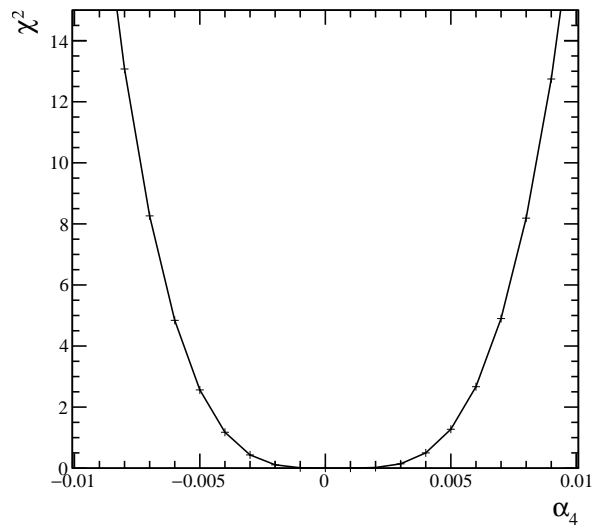


Figure 1.8.: χ^2 as a function of α_4 assuming $\alpha_5 = 0$ for the $qqqq\nu\nu$ final state arising from a fit to $\cos\theta_{\text{jets}}^*$ at 1.4 TeV for the optimal jet reconstruction parameters.

| PFO Selection | Tight Selected PFOs | Selected PFOs | Loose Selected PFOs |
|---------------|----------------------|----------------------|----------------------|
| R Parameter | | | |
| 0.7 | -0.0039 ± 0.0050 | -0.0038 ± 0.0050 | -0.0037 ± 0.0046 |
| 0.9 | -0.0041 ± 0.0051 | -0.0038 ± 0.0046 | -0.0038 ± 0.0048 |
| 1.1 | -0.0041 ± 0.0051 | -0.0039 ± 0.0050 | -0.0040 ± 0.0050 |

Table 1.3.: Precision on measurement of α_4 at 1.4 TeV for different jet reconstruction parameters considering pure signal and applying a χ^2 fit to $\cos\theta_{jets}^*$.

| PFO Selection | Tight Selected PFOs | Selected PFOs | Loose Selected PFOs |
|---------------|----------------------|----------------------|----------------------|
| R Parameter | | | |
| 0.7 | -0.0027 ± 0.0031 | -0.0027 ± 0.0032 | -0.0025 ± 0.0030 |
| 0.9 | -0.0028 ± 0.0032 | -0.0026 ± 0.0030 | -0.0026 ± 0.0030 |
| 1.1 | -0.0028 ± 0.0032 | -0.0027 ± 0.0032 | -0.0028 ± 0.0031 |

Table 1.4.: Precision on measurement of α_5 at 1.4 TeV for different jet reconstruction parameters considering pure signal and applying a χ^2 fit to $\cos\theta_{jets}^*$.

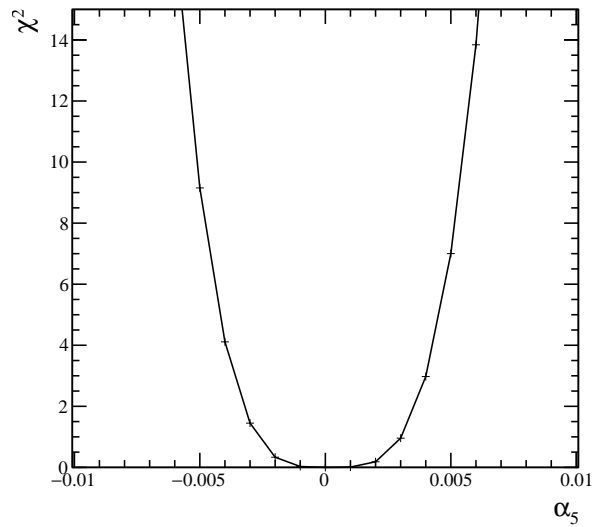


Figure 1.9.: χ^2 as a function of α_5 assuming $\alpha_4 = 0$ for the $qqqq\nu\nu$ final state arising from a fit to $\cos\theta_{jets}^*$ at 1.4 TeV for the optimal jet reconstruction parameters.

| PFO Selection | Tight Selected PFOs | Selected PFOs | Loose Selected PFOs |
|---------------|--------------------------|--------------------------|--------------------------|
| R Parameter | | | |
| 0.7 | -0.00051 ± 0.000508 | -0.000477 ± 0.000487 | -0.000531 ± 0.000539 |
| 0.9 | -0.000548 ± 0.000541 | -0.000519 ± 0.000505 | -0.000550 ± 0.000539 |
| 1.1 | -0.000446 ± 0.00045 | -0.000481 ± 0.000466 | -0.000478 ± 0.000467 |

Table 1.5.: Precision on measurement of α_4 at 3 TeV for different jet reconstruction parameters considering pure signal and applying a χ^2 fit to $\cos\theta_{jets}^*$.

| PFO Selection | Tight Selected PFOs | Selected PFOs | Loose Selected PFOs |
|---------------|--------------------------|--------------------------|--------------------------|
| R Parameter | | | |
| 0.7 | -0.000375 ± 0.000358 | -0.000350 ± 0.000343 | -0.000346 ± 0.00034 |
| 0.9 | -0.000378 ± 0.000355 | -0.000376 ± 0.000351 | -0.000379 ± 0.000358 |
| 1.1 | -0.000339 ± 0.000328 | -0.000358 ± 0.000343 | -0.000339 ± 0.000326 |

Table 1.6.: Precision on measurement of α_5 at 3 TeV for different jet reconstruction parameters considering pure signal and applying a χ^2 fit to $\cos\theta_{jets}^*$.

1.8. Event Selection

As discussed earlier the signal events for this analysis contain the $\nu\nu qqqq$ final state. The processes to be considered in this analysis alongside the signal are events that would topologically look similar to signal in the detector. This includes events that could be confused with 4 jet events with missing energy, while excluding those events with large numbers of high energy leptons that could be vetoed easily during the analysis stage. In full the list includes:

EPA (equivalent photon approximation) processes models interactions of the electric field of the incoming electrons and positrons with their corresponding antiparticles at the collision point. In such interactions the electric fields of the charged particles are approximated as photons hence the name. The beamstrahlung processes model the collision of a photon radiated off a charged particle with the corresponding bunch incoming lepton. Photons are radiated from the incoming charged leptons as the bunches carrying the leptons are very small producing very large electromagnetic fields. Interactions with the charged leptons and these fields yields the beamstrahlung photons. The energy spectrum of the incoming particles for CLIC at the relevant

| Final State | Cross Section 1.4 TeV [fb] | Cross Section 3 TeV [fb] |
|---|----------------------------|--------------------------|
| $e^+e^- \rightarrow \nu\nu qqqq$ | 24.7 | 71.5 |
| $e^+e^- \rightarrow l\nu qqqq$ | 110.4 | 106.6 |
| $e^+e^- \rightarrow ll qqqq$ | 62.1 | 169.3 |
| $e^+e^- \rightarrow qqqq$ | 1245.1 | 546.5 |
| $e^+e^- \rightarrow \nu\nu qq$ | 787.7 | 546.5 |
| $e^+e^- \rightarrow l\nu qq$ | 4309.7 | 5560.9 |
| $e^+e^- \rightarrow ll qq$ | 2725.8 | 3319.6 |
| $e^+e^- \rightarrow qq$ | 4009.5 | 2948.9 |
| $\gamma_{\text{EPA}}e^- \rightarrow qqqqe^-$ | 287.1 | 287.8 |
| $\gamma_{\text{BS}}e^- \rightarrow qqqqe^-$ | 1160.7 | 1268.6 |
| $e^+\gamma_{\text{EPA}} \rightarrow qqqqe^+$ | 286.9 | 287.8 |
| $e^+\gamma_{\text{BS}} \rightarrow qqqqe^+$ | 1156.3 | 1267.3 |
| $\gamma_{\text{EPA}}e^- \rightarrow qqqq\nu$ | 32.6 | 54.2 |
| $\gamma_{\text{BS}}e^- \rightarrow qqqq\nu$ | 136.9 | 262.5 |
| $e^+\gamma_{\text{EPA}} \rightarrow qqqq\nu$ | 32.6 | 54.2 |
| $e^+\gamma_{\text{BS}} \rightarrow qqqq\nu$ | 136.4 | 262.3 |
| $\gamma_{\text{EPA}}\gamma_{\text{EPA}} \rightarrow qqqq$ | 753.0 | 402.7 |
| $\gamma_{\text{EPA}}\gamma_{\text{BS}} \rightarrow qqqq$ | 4034.8 | 2423.1 |
| $\gamma_{\text{BS}}\gamma_{\text{EPA}} \rightarrow qqqq$ | 4018.7 | 2420.6 |
| $\gamma_{\text{BS}}\gamma_{\text{BS}} \rightarrow qqqq$ | 21406.2 | 13050.3 |

Table 1.7.: Cross sections of signal and background processes at 1.4 and 3 TeV. In the above table $q \in u, \bar{u}, d, \bar{d}, s, \bar{s}, c, \bar{c}, b$ or \bar{b} while $l \in e^\pm, \mu^\pm$ or τ^\pm and $\nu \in \nu_e, \nu_\mu$ and ν_τ . The subscript EPA or BS for the incoming photons indicate whether the photon is generated from the equivalent photon approximation or beamstrahlung.

operating energy is used to model the energy of the incoming photons. Included in these cases are the photon-photon interactions from photons appearing from the EPA and beamstrahlung processes.

The dominant beam related background processes at CLIC are as follows:

- e^+e^- pair creation from the interaction of a beamstrahlung photon with the electromagnetic field from the opposite beam. The different mechanisms for pair creation are coherent, incoherent and trident pairs are pair production. Coherent pair production occurs when a real beamstrahlung photon interacts with the electromagnetic field from the opposite beam, trident pair production occurs

when a virtual beamstrahlung photon interacts with the electromagnetic field from the opposite beam and incoherent pair production occur when a real or virtual beamstrahlung photon interacts with the individual particles in the opposite beam.

- $\gamma\gamma \rightarrow \text{Hadron}$ from the interaction of beamstrahlung photons with each other and or the electric field of charged particles in the opposite beam that may appear as virtual photons. Example Feynman diagrams for such processes is shown in figure ??.
- Beam halo muons that arise from inelastic collisions of the beam particles during collimation.

These have to be properly addressed to get a true measure of the physics potential at CLIC. As figure 1.10 shows the transverse momentum of coherent and trident pair produced e^+e^- is sufficiently small that a transverse momentum cut is enough to remove the vast majority of these particles. This is not the case however for incoherent pair production e^+e^- and $\gamma\gamma \rightarrow \text{Hadron}$.

HERE

Unlike the majority the other major background processes for the CLIC experiment [8], those of incoherent pair production of e^+e^- pairs from beamstrahlung photons and beam halo muons from interactions of the beam with particles outside the detector, the $\gamma\gamma \rightarrow \text{Hadron}$ processes have a large transverse momentum and cannot be vetoed with a simple transverse momentum cut as shown in figure .

To account for this non negligible background $\gamma\gamma \rightarrow \text{Hadron}$ events are overlaid onto CLIC samples. The number of events overlaid per event is drawn from a Poisson with a mean of 3.2 for 3 TeV and 1.3 for 1.4 TeV samples. The PFO choices described in section 1.7 are applied to veto PFOs that arise from these overlaid background events.

1.8.1. Pre Selection - 1.4 TeV

The primary selection of the $\nu\nu qqqq$ signal will be done using a multivariate analysis, however, in an attempt to veto trivial backgrounds a simple cut based preselection is applied. Cuts are applied to the transverse momentum, invariant mass of the visible system and the number of isolated leptons. The raw distributions of these variables is

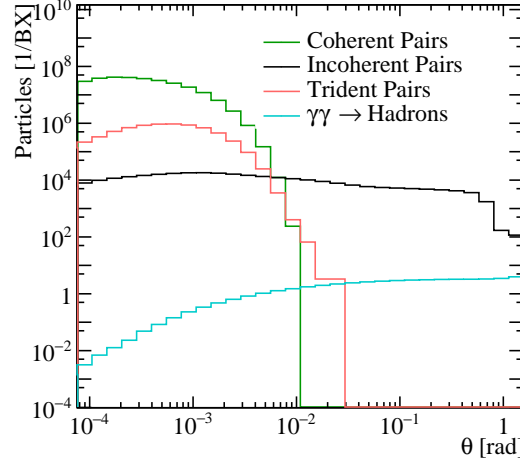


Figure 1.10.: Angular distribution of number of particles for beam induced backgrounds for CLIC at $\sqrt{s} = 3$ TeV. Taken from CLIC CDR.

shown in figures 1.11, 1.12 and 1.13. Based on these distributions the following cuts were applied:

- Transverse momentum > 100 GeV. This cut is effective due to the presence of missing energy in the form of neutrinos in the signal final state.
- Visible mass of the system > 200 GeV. This cut is effective for accounting for the missing energy of the neutrinos in the final state along the longitudinal direction of the detector instead.
- Number of isolated leptons = 0. This cut vetos a large number of events with leptons in the final state. The effect of these preselection cuts can be found in table 1.3. While a large fraction of the signal events are lost through these cuts, particularly the transverse momentum cuts, a much large fraction of background events are removed justifying the cut.

The event numbers for the signal and background are shown in table 1.8 as these cuts are cumulatively applied. These numbers are normalised to the correct luminosity for CLIC running at 1.4 TeV.

As referenced in section <- Iso lep finder good at vetoing other sensitive events

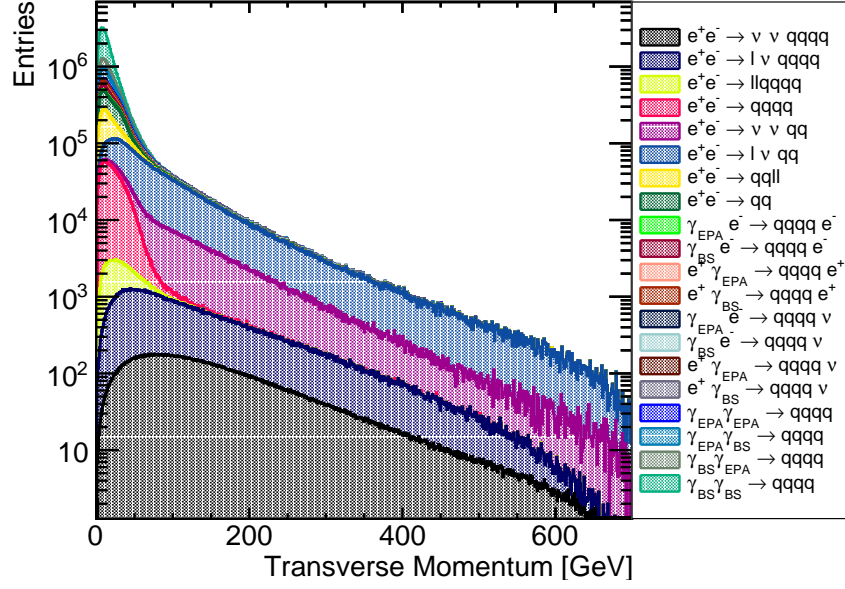


Figure 1.11.: The transverse momentum of signal and background events at 1.4 TeV.

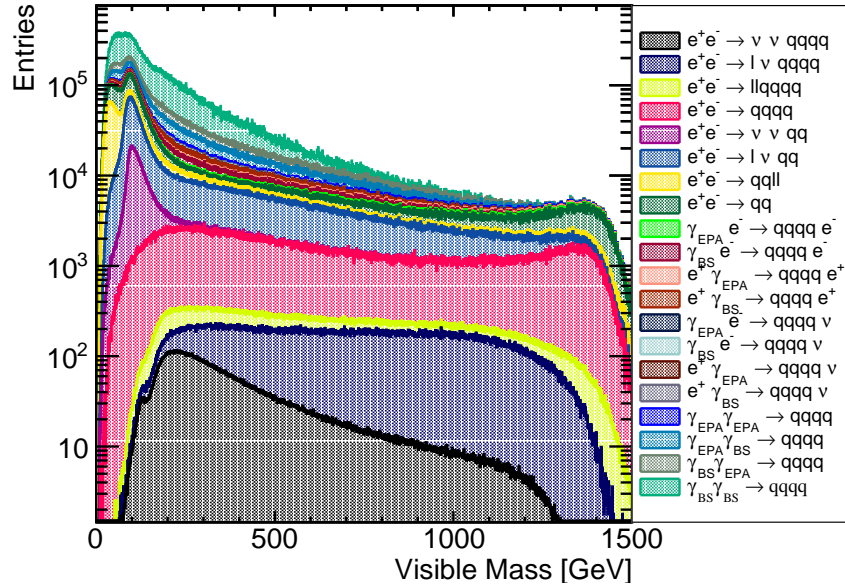


Figure 1.12.: The invariant mass of the visible system of signal and background events at 1.4 TeV.

| Final State | Raw Event Numbers | $p_T > 100$ GeV | $p_T > 100$ GeV & $M_{\text{Vis}} > 200$ GeV | $p_T > 100$ GeV & $M_{\text{Vis}} > 200$ GeV & $N_{\text{Isolated Leptons}} = 0$ |
|--|----------------------|-----------------|---|--|
| $e^+e^- \rightarrow \nu\nu qqqq$ | 37,050 | 23,782 | 21,091 | 21,034 |
| $e^+e^- \rightarrow l\nu qqqq$ | 165,600 | 81,631 | 80,827 | 42,332 |
| $e^+e^- \rightarrow ll qqqq$ | 93,150 | 1,154 | 1,142 | 710 |
| $e^+e^- \rightarrow qq qq$ | 1,867,631 | 6,755 | 6,742 | 6,729 |
| $e^+e^- \rightarrow \nu\nu qq$ | 1,181,218 | 514,701 | 49,692 | 49,586 |
| $e^+e^- \rightarrow l\nu qq$ | 6,463,852 | 2,002,405 | 1,258,172 | 568,450 |
| $e^+e^- \rightarrow ll qq$ | 4,088,143 | 7,656 | 7,263 | 5,651 |
| $e^+e^- \rightarrow qq$ | 6,010,154 | 34,123 | 33,679 | 33,605 |
| $\gamma_{\text{EPA}}e^- \rightarrow qq qq e^-$ | 430,643 | 2,301 | 2,294 | 762 |
| $\gamma_{\text{BS}}e^- \rightarrow qq qq e^-$ | 1,741,050 | 1,773 | 1,688 | 1,294 |
| $e^+\gamma_{\text{EPA}} \rightarrow qq qq e^+$ | 430,344 | 2,787 | 2,774 | 1,057 |
| $e^+\gamma_{\text{BS}} \rightarrow qq qq e^+$ | 1,734,450 | 814 | 784 | 552 |
| $\gamma_{\text{EPA}}e^- \rightarrow qq qq \nu$ | 48,893 | 17,468 | 13,558 | 8,895 |
| $\gamma_{\text{BS}}e^- \rightarrow qq qq \nu$ | 205,326 | 75,429 | 48,648 | 48,023 |
| $e^+\gamma_{\text{EPA}} \rightarrow qq qq \nu$ | 48,893 | 17,656 | 13,588 | 8,951 |
| $e^+\gamma_{\text{BS}} \rightarrow qq qq \nu$ | 204,581 | 74,890 | 48,457 | 47,903 |
| $\gamma_{\text{EPA}}\gamma_{\text{EPA}} \rightarrow qq qq$ | 1,129,459 | 3,126 | 3,018 | 1,421 |
| $\gamma_{\text{EPA}}\gamma_{\text{BS}} \rightarrow qq qq$ | 6,052,200 | 7,205 | 7,059 | 5,531 |
| $\gamma_{\text{BS}}\gamma_{\text{EPA}} \rightarrow qq qq$ | 6,027,979 | 5,187 | 5,116 | 3,197 |
| $\gamma_{\text{BS}}\gamma_{\text{BS}} \rightarrow qq qq$ | 32,109,300 | 4,421 | 4,421 | 3,617 |

Table 1.8.: Number of events passing the various cuts applied in the preselection at 1.4TeV. Event numbers are normalised to the correct luminosity for CLIC at 1.4 TeV. p_T is the transverse momentum of the event, M_{Vis} is the visible mass and $N_{\text{Isolated Leptons}}$ is the number of isolated leptons in the event. In the above table $q \in u, \bar{u}, d, \bar{d}, s, \bar{s}, c, \bar{c}, b, \bar{b}$ while $l \in e^\pm, \mu^\pm$ or τ^\pm and $\nu \in \nu_e, \nu_\mu$ and ν_τ . The subscript EPA or BS for the incoming photons indicate whether the photon is generated from the equivalent photon approximation or beamstrahlung.

1.8.2. MVA - 1.4 TeV

A multivariate analysis was applied to the data set to refine the selection using the TMVA toolkit [6]. The following variables were used for training the TMVA selection.

- Number of PFOs in the event.

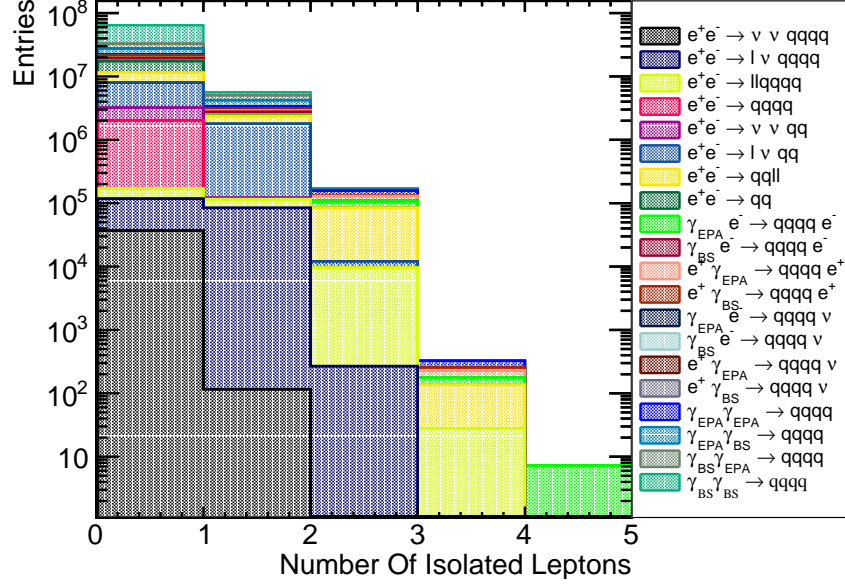


Figure 1.13.: The number of isolated leptons for signal and background events at 1.4 TeV.

- Highest energy PFO type.
- Transverse momentum of the event.
- $\cos\theta_{Missing}$. The cosine of the polar angle of the missing momentum.
- $\cos\theta_{Highest\ Energy\ Track}$. The cosine of the polar angle of the track with the largest momentum.
- y_i, y_{i+1} . Jet clustering parameters ranging from $i = 0$ to 6.
- Principle thrust, sphericity and aplanarity as defined in section BLAH.
- Energy of the highest energy electron in the event.
- Energy of the highest energy PFO in the event.
- Energy of the reconstructed bosons.
- Acolinearity of the reconstructed boson pair.
- Invariant mass of the reconstructed bosons.
- Acolinearity of the jets forming the reconstructed bosons.

It was found that the best MVA algorithm for both performance and speed was the booted decision tree (BDT) when comparing different methods using the default settings. Add plot here.

The BDT was further optimised by varying the number of trees used, the depth of the trees and the number of cuts applied. The results shown in the rest of this section use the optimal configuration. For the optimal BDT configuration a significance of $S/\sqrt{(S+B)} = 49.7$ was obtained.

The event numbers passing the BDT cut can be found in table 1.9. The performance of the BDT is shown in figure 1.14, which shows the change in the distribution of the the invariant mass of the reconstructed bosons as the MVA is applied. As expected the dominant background processes after the MVA is applied are those that will look identical to the visible signal process i.e. $qqqq$ and missing energy. Two smaller sources of background that pass the MVA exists, those where two jets and missing energy are confused as four jets and missing energy and those where a lepton is not properly reconstructed and the events look like four jets and missing energy.

1.8.3. Pre Selection - 3 TeV

1.8.4. MVA - 3 TeV

1.9. Fit

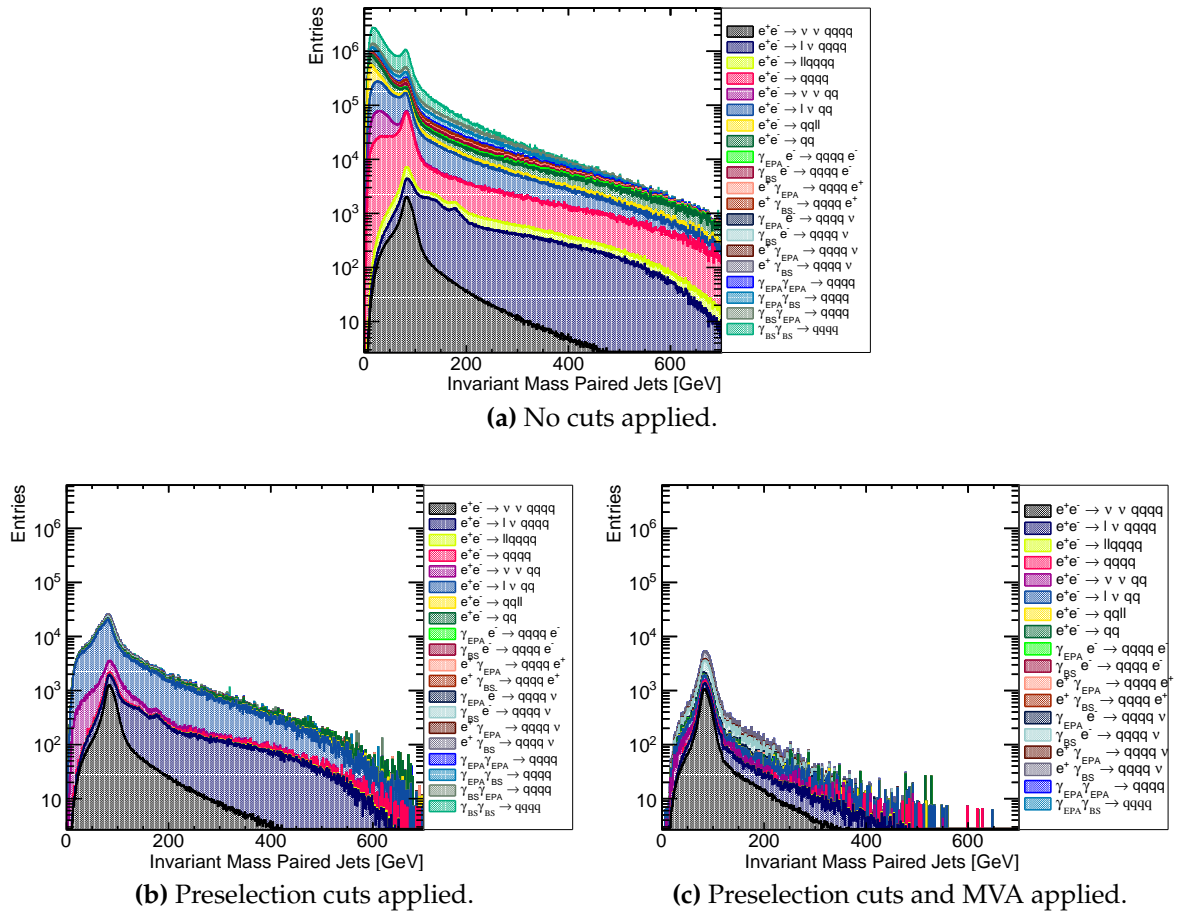


Figure 1.14.: Impact of preselection and MVA on the reconstructed invariant mass of the bosons arising from jet pairing at 1.4 TeV.

| Final State | Raw Event Numbers | Post MVA Selection Numbers |
|---|-------------------|----------------------------|
| $e^+e^- \rightarrow \nu\nu qqqq$ | 37,050 | 15,167 |
| $e^+e^- \rightarrow l\nu qqqq$ | 165,600 | 6,744 |
| $e^+e^- \rightarrow ll qqqq$ | 93,150 | 90 |
| $e^+e^- \rightarrow qqqq$ | 1,867,631 | 1,417 |
| $e^+e^- \rightarrow \nu\nu qq$ | 1,181,218 | 3,648 |
| $e^+e^- \rightarrow l\nu qq$ | 6,463,852 | 7,169 |
| $e^+e^- \rightarrow ll qq$ | 4,088,143 | 296 |
| $e^+e^- \rightarrow qq$ | 6,010,154 | 1,184 |
| $\gamma_{\text{EPA}}e^- \rightarrow qqqqe^-$ | 430,643 | 27 |
| $\gamma_{\text{BS}}e^- \rightarrow qqqqe^-$ | 1,741,050 | 113 |
| $e^+\gamma_{\text{EPA}} \rightarrow qqqqe^+$ | 430,344 | 25 |
| $e^+\gamma_{\text{BS}} \rightarrow qqqqe^+$ | 1,734,450 | 58 |
| $\gamma_{\text{EPA}}e^- \rightarrow qqqq\nu$ | 48,893 | 3,728 |
| $\gamma_{\text{BS}}e^- \rightarrow qqqq\nu$ | 205,326 | 25,723 |
| $e^+\gamma_{\text{EPA}} \rightarrow qqqq\nu$ | 48,893 | 3,776 |
| $e^+\gamma_{\text{BS}} \rightarrow qqqq\nu$ | 204,581 | 25,842 |
| $\gamma_{\text{EPA}}\gamma_{\text{EPA}} \rightarrow qqqq$ | 1,129,459 | 81 |
| $\gamma_{\text{EPA}}\gamma_{\text{BS}} \rightarrow qqqq$ | 6,052,200 | 73 |
| $\gamma_{\text{BS}}\gamma_{\text{EPA}} \rightarrow qqqq$ | 6,027,979 | 0 |
| $\gamma_{\text{BS}}\gamma_{\text{BS}} \rightarrow qqqq$ | 32,109,300 | 0 |

Table 1.9.: Number of events passing the MVA selection at 1.4TeV. Event numbers are normalised to the correct luminosity for CLIC at 1.4 TeV. The subscript EPA or BS for the incoming photons indicate whether the photon is generated from the equivalent photon approximation or beamstrahlung.

Appendix A.

Pointless extras

*“Le savant n’étudie pas la nature parce que cela est utile;
il l’étudie parce qu’il y prend plaisir,
et il y prend plaisir parce qu’elle est belle.”*
— Henri Poincaré, 1854–1912

Appendixes (or should that be “appendices”?) make you look really clever, ‘cos it’s like you had more clever stuff to say than could be fitted into the main bit of your thesis. Yeah. So everyone should have at least three of them...

A.1. Anomalous Gauge Coupling Quartic Vertices Of Relevance in Vector Boson Scattering

The anomalous gauge couplings involving α_4 and α_5 arise in EFT through the addition of the following terms to the Lagrangian.

$$\text{Tr}(V^\mu V_\nu) \text{Tr}(V^\nu V_\mu) \text{ and } [\text{Tr}(V^\mu V_\mu)]^2 \quad (\text{A.1})$$

Where V_μ is defined in the following way.

$$V_\mu = \Sigma(D_\mu \Sigma)^\dagger \quad (\text{A.2})$$

and Σ , the Higgs field matrix, is defined as.

$$\Sigma = \exp\left(-\frac{i}{v}\mathbf{w}\right) \quad (\text{A.3})$$

Where $\mathbf{w} = w^a \sigma^a$. w^a are the ... and σ^a are the Pauli spin matrices. The covariant derivative of the Higgs field matrix is

$$D_\mu \Sigma = (\partial_\mu + \frac{ig}{2}W_\mu - \frac{ig'}{2}B_\mu \sigma^3)\Sigma \quad (\text{A.4})$$

For clarity consider the unitarity gauge where $\mathbf{w} = 0$, which implies $\Sigma = 1$. In this gauge V_μ takes the following form.

$$\begin{aligned} V_\mu &= \frac{i}{2}(gW_\mu^i \sigma^i - g'B_\mu \sigma^3) = \frac{i}{2} \begin{pmatrix} gW_\mu^3 - g'B_\mu & g(W_\mu^1 - iW_\mu^2) \\ g(W_\mu^1 + iW_\mu^2) & -gW_\mu^3 + g'B_\mu \end{pmatrix} \\ &= \frac{i}{2} \begin{pmatrix} \sqrt{g^2 + g'^2}Z_\mu & g\sqrt{2}W_\mu^+ \\ g\sqrt{2}W_\mu^- & \sqrt{g^2 + g'^2}Z_\mu \end{pmatrix} \end{aligned}$$

Where the relationship between the mass and gauge symmetry basis are as follows.

$$W_\mu^+ = \frac{1}{\sqrt{2}}(W_\mu^1 - iW_\mu^2) \quad (\text{A.5})$$

$$W_\mu^- = \frac{1}{\sqrt{2}}(W_\mu^1 + iW_\mu^2) \quad (\text{A.6})$$

$$Z_\mu = c_w W_\mu^3 - s_w B_\mu \quad (\text{A.7})$$

$$A_\mu = s_w W_\mu^3 + c_w B_\mu \quad (\text{A.8})$$

With $c_w = \frac{g}{\sqrt{g^2 + g'^2}}$ and $s_w = \frac{g'}{\sqrt{g^2 + g'^2}}$. Consider the expansion of the terms to be included in the Lagrangian.

$$V^\mu V_\nu = \frac{-1}{4} \begin{pmatrix} \sqrt{g^2 + g'^2} Z^\mu & g\sqrt{2} W^{+\mu} \\ g\sqrt{2} W^{-\mu} & \sqrt{g^2 + g'^2} Z^\mu \end{pmatrix} \begin{pmatrix} \sqrt{g^2 + g'^2} Z_\nu & g\sqrt{2} W_\nu^+ \\ g\sqrt{2} W_\nu^- & \sqrt{g^2 + g'^2} Z_\nu \end{pmatrix} \quad (\text{A.9})$$

$$\text{Tr}[V^\mu V_\nu] = \frac{-1}{2} ((g^2 + g'^2) Z^\mu Z_\nu + g^2 W^{+\mu} W_\nu^- + g^2 W^{-\mu} W_\nu^+) \quad (\text{A.10})$$

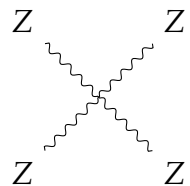
$$\text{Tr}[V^\mu V_\nu] \text{Tr}[V_\mu V^\nu] = \frac{(g^2 + g'^2)^2}{4} (Z^\mu Z_\mu)^2 + g^2 (g^2 + g'^2) (Z^\mu Z^\nu W_\mu^- W_\nu^+) \quad (\text{A.11})$$

$$+ \frac{g^4}{2} (W^{-\mu} W_\mu^+)^2 + \frac{g^4}{2} (W^{-\mu} W^{+\nu} W_\mu^- W_\nu^+) \quad (\text{A.12})$$

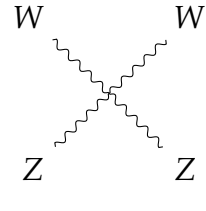
$$\text{Tr}[V^\mu V_\mu]^2 = \frac{(g^2 + g'^2)^2}{4} (Z^\mu Z_\mu)^2 + g^2 (g^2 + g'^2) (Z^\mu Z^\nu W_\mu^- W_\nu^+) \quad (\text{A.13})$$

$$+ g^4 (W^{-\mu} W_\mu^+)^2 \quad (\text{A.14})$$

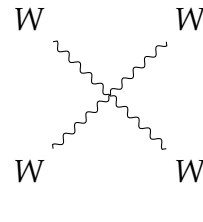
These two terms change the cross section for the vector boson scattering processes at CLIC that involve $ZZ \rightarrow ZZ$, $W^+ W^- \rightarrow ZZ$, $ZZ \rightarrow W^+ W^-$ and $W^+ W^- \rightarrow W^+ W^-$.



$$\subset (\alpha_4 + \alpha_5) \frac{(g^2 + g'^2)^2}{4} \quad (\text{A.15})$$



$$\subset (\alpha_4 + \alpha_5)g^2(g^2 + g'^2) \quad (\text{A.16})$$



$$\subset (\alpha_4 + 2\alpha_5)\frac{g^4}{2} \text{ and } \frac{g^4}{2}\alpha_4 \quad (\text{A.17})$$

A.2. χ^2 Contour Plots for Jet Algorithm Optimisation

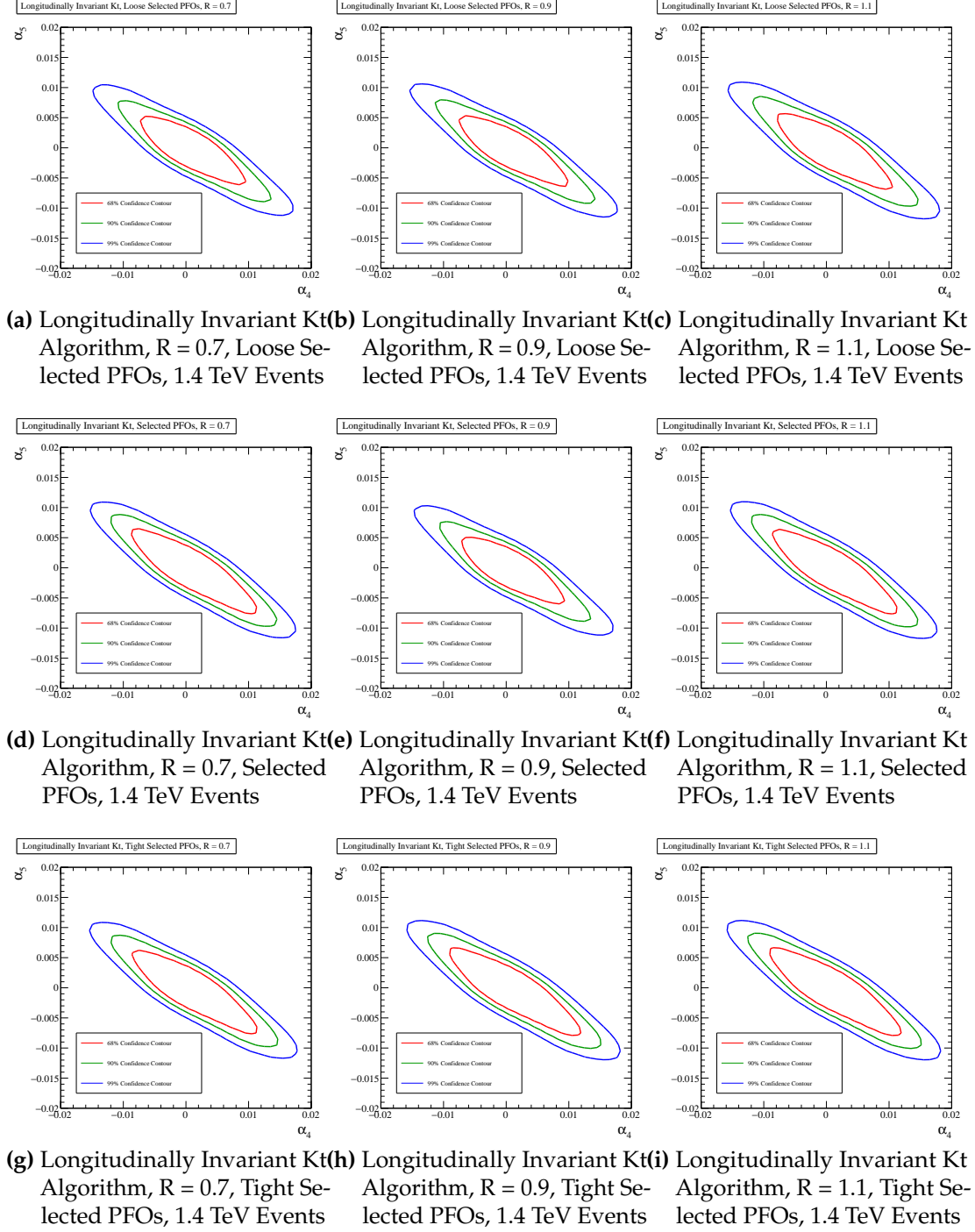


Figure A.1.: χ^2 Sensitivity contours for the $qqqq\nu\nu$ final state arising from a fit to $\cos\theta_{\text{jets}}^*$ at 1.4 TeV for different values of jet reconstruction parameters.

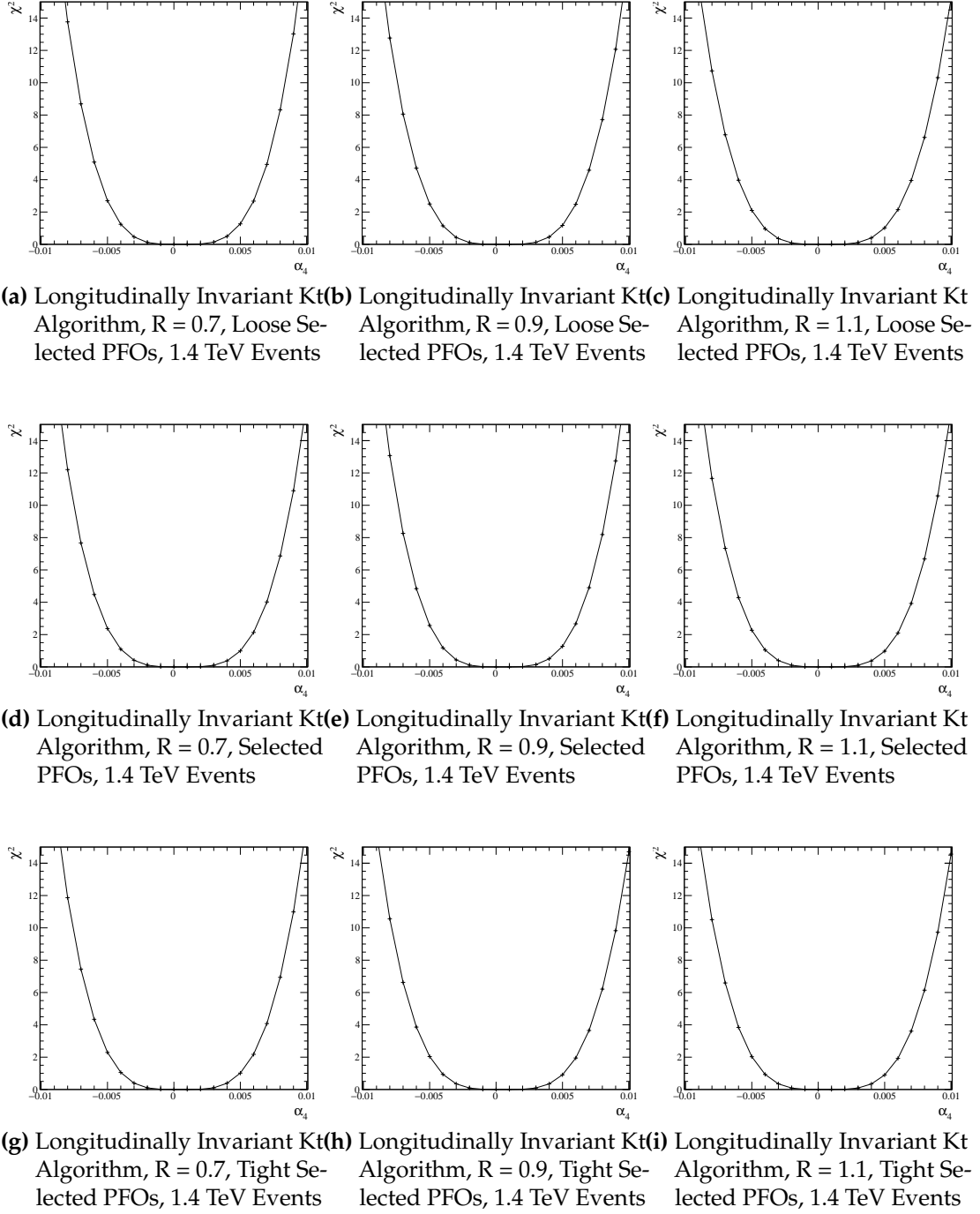


Figure A.2.: χ^2 as a function of α_4 assuming $\alpha_5 = 0$ for the $qqqq\nu\nu$ final state arising from a fit to $\cos\theta_{\text{jets}}^*$ at 1.4 TeV for different values of jet reconstruction parameters.

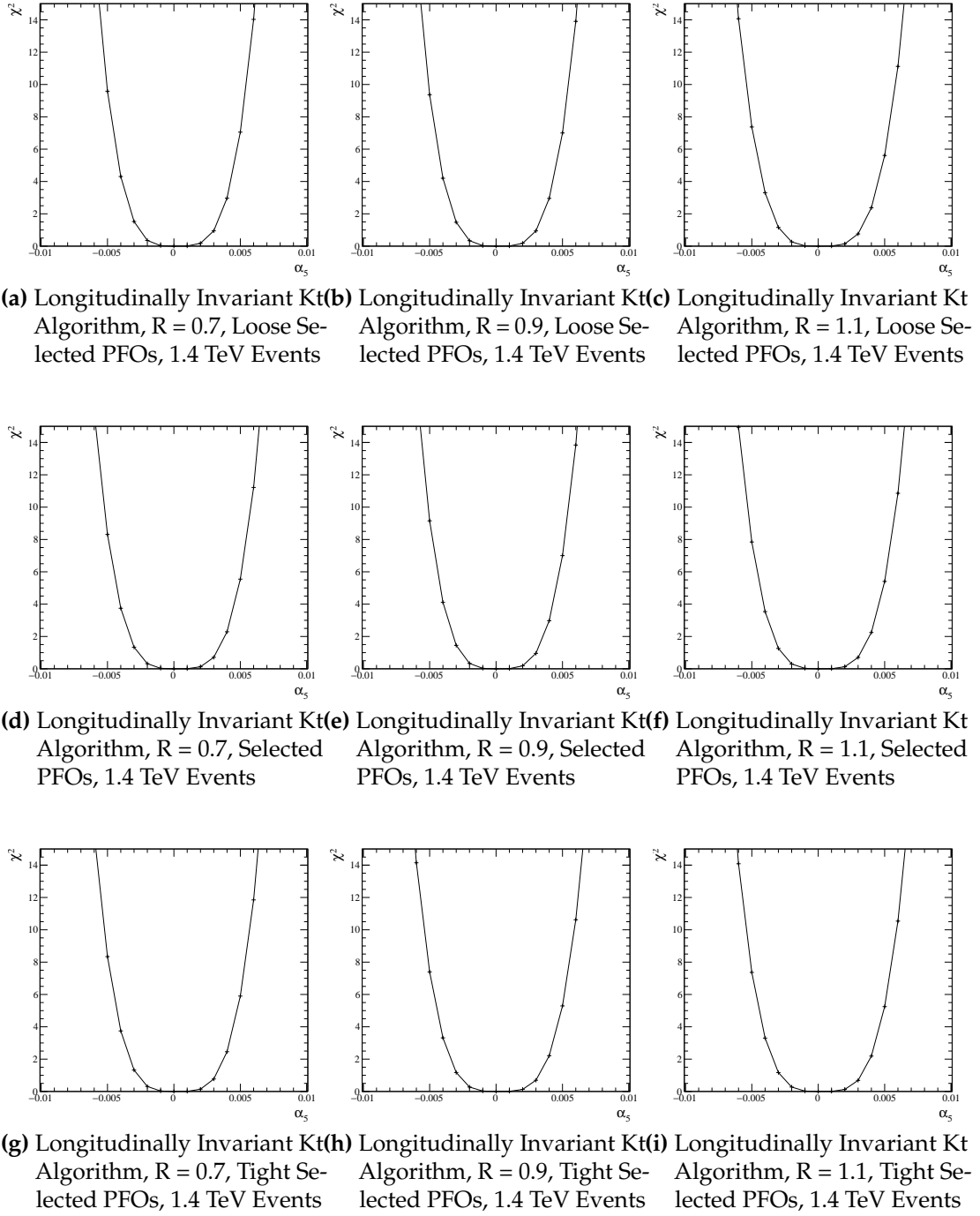
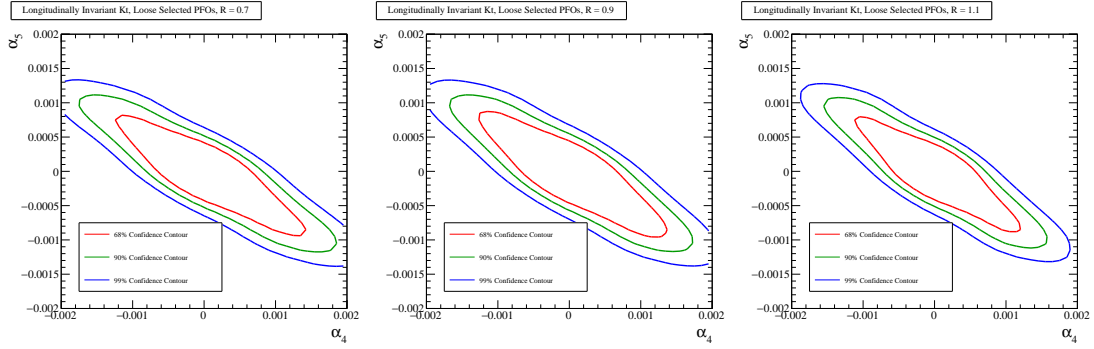


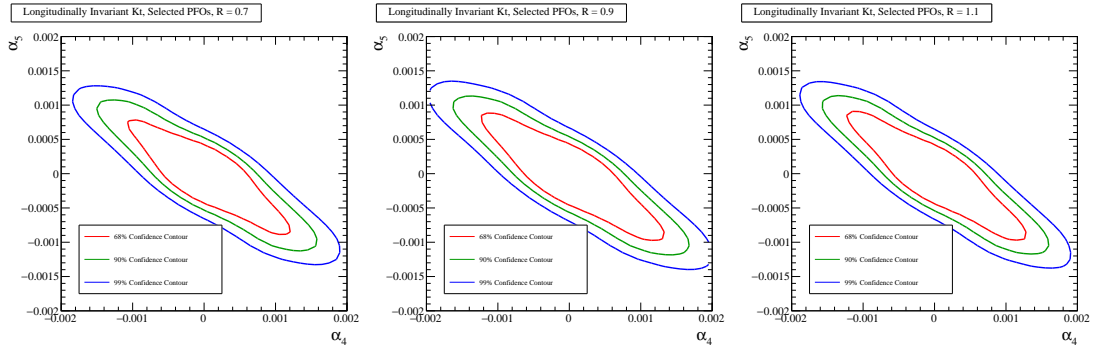
Figure A.3.: χ^2 as a function of α_5 assuming $\alpha_4 = 0$ for the $qqqq\nu\nu$ final state arising from a fit to $\cos\theta_{\text{jets}}^*$ at 1.4 TeV for different values of jet reconstruction parameters.



(a) Longitudinally Invariant Kt Algorithm, $R = 0.7$, Loose Selected PFOs, 3 TeV Events

(b) Longitudinally Invariant Kt Algorithm, $R = 0.9$, Loose Selected PFOs, 3 TeV Events

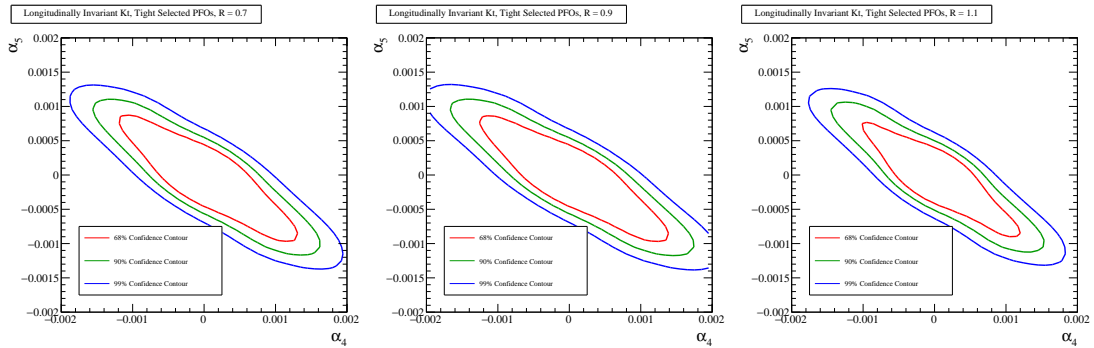
(c) Longitudinally Invariant Kt Algorithm, $R = 1.1$, Loose Selected PFOs, 3 TeV Events



(d) Longitudinally Invariant Kt Algorithm, $R = 0.7$, Selected PFOs, 3 TeV Events

(e) Longitudinally Invariant Kt Algorithm, $R = 0.9$, Selected PFOs, 3 TeV Events

(f) Longitudinally Invariant Kt Algorithm, $R = 1.1$, Selected PFOs, 3 TeV Events



(g) Longitudinally Invariant Kt Algorithm, $R = 0.7$, Tight Selected PFOs, 3 TeV Events

(h) Longitudinally Invariant Kt Algorithm, $R = 0.9$, Tight Selected PFOs, 3 TeV Events

(i) Longitudinally Invariant Kt Algorithm, $R = 1.1$, Tight Selected PFOs, 3 TeV Events

Colophon

This thesis was made in $\text{\LaTeX}2_{\epsilon}$ using the “hepthesis” class [3].

Bibliography

- [1] Toshinori Abe et al. The International Large Detector: Letter of Intent. 2010, 1006.3396.
- [2] S. Agostinelli et al. GEANT4: A Simulation toolkit. *Nucl. Instrum. Meth.*, A506:250–303, 2003.
- [3] Andy Buckley. The hepthesis L^AT_EX class.
- [4] Matteo Cacciari, Gavin P. Salam, and Gregory Soyez. FastJet User Manual. *Eur. Phys. J.*, C72:1896, 2012, 1111.6097.
- [5] F. Gaede. Marlin and LCCD: Software tools for the ILC. *Nucl. Instrum. Meth.*, A559:177–180, 2006.
- [6] Andreas Hoecker, Peter Speckmayer, Joerg Stelzer, Jan Therhaag, Eckhard von Toerne, and Helge Voss. TMVA: Toolkit for Multivariate Data Analysis. *PoS, ACAT:040*, 2007, physics/0703039.
- [7] Wolfgang Kilian, Thorsten Ohl, and Jurgen Reuter. WHIZARD: Simulating Multi-Particle Processes at LHC and ILC. *Eur. Phys. J.*, C71:1742, 2011, 0708.4233.
- [8] Lucie Linssen, Akiya Miyamoto, Marcel Stanitzki, and Harry Weerts. Physics and Detectors at CLIC: CLIC Conceptual Design Report. 2012, 1202.5940.
- [9] J. S. Marshall, A. M \ddot{a} ijnnich, and M. A. Thomson. Performance of Particle Flow Calorimetry at CLIC. *Nucl. Instrum. Meth.*, A700:153–162, 2013, 1209.4039.
- [10] P. Mora de Freitas and H. Videau. Detector simulation with MOKKA / GEANT4: Present and future. In *Linear colliders. Proceedings, International Workshop on physics and experiments with future electron-positron linear colliders, LCWS 2002, Seogwipo, Jeju Island, Korea, August 26-30, 2002*, pages 623–627, 2002.
- [11] Mauro Moretti, Thorsten Ohl, and Jurgen Reuter. O’Mega: An Optimizing matrix

element generator. 2001, hep-ph/0102195.

- [12] Taikan Suehara and Tomohiko Tanabe. LCFIPlus: A Framework for Jet Analysis in Linear Collider Studies. *Nucl. Instrum. Meth.*, A808:109–116, 2016, 1506.08371.
- [13] M. A. Thomson. Particle Flow Calorimetry and the PandoraPFA Algorithm. *Nucl. Instrum. Meth.*, A611:25–40, 2009, 0907.3577.

List of figures

| | |
|--|----|
| 1.1. Event weights from Whizard for 1.4TeV $\nu\nu qqqq$ final state events. . . . | 4 |
| 1.2. Comparison of various distributions between samples used in this analysis and the official CLIC samples for the $\nu\nu qqqq$ final state. | 6 |
| 1.3. Reconstructed invariant masses for different choices of jet algorithm for 1.4 TeV and 3 TeV $\nu\nu qqqq$ events. | 8 |
| 1.4. Sensitivity of $\cos\theta_{jets}^8$ to the anomalous gauge couplings α_4 and α_5 at 1.4 and 3 TeV. | 12 |
| 1.5. Sensitivity of $\cos\theta_{Bosons}^8$ to the anomalous gauge couplings α_4 and α_5 at 1.4 and 3 TeV. | 12 |
| 1.6. Event weights from Whizard for 1.4TeV $\nu\nu qqqq$ final state events with interpolated surface. | 13 |
| 1.7. χ^2 Sensitivity contours for the $qqqq\nu\nu$ final state arising from a fit to $\cos\theta_{jets}^*$ at 1.4 TeV for the optimal jet reconstruction parameters. | 15 |
| 1.8. χ^2 as a function of α_4 assuming $\alpha_5 = 0$ for the $qqqq\nu\nu$ final state arising from a fit to $\cos\theta_{jets}^*$ at 1.4 TeV for the optimal jet reconstruction parameters. | 15 |
| 1.9. χ^2 as a function of α_5 assuming $\alpha_4 = 0$ for the $qqqq\nu\nu$ final state arising from a fit to $\cos\theta_{jets}^*$ at 1.4 TeV for the optimal jet reconstruction parameters. | 16 |
| 1.11. Transverse momentum at 1.4 TeV. | 21 |
| 1.12. Invariant mass of the visible system at 1.4 TeV. | 21 |
| 1.13. Number of isolated leptons at 1.4 TeV. | 23 |

| | |
|---|----|
| 1.14. Impact of preselection and MVA on the reconstructed invariant mass of the bosons arising from jet pairing at 1.4 TeV. | 25 |
| A.1. χ^2 Sensitivity contours for the $qqqq\nu\nu$ final state arising from a fit to $\cos\theta_{\text{jets}}^*$ at 1.4 TeV for different values of jet reconstruction parameters. | 31 |
| A.2. χ^2 as a function of α_4 assuming $\alpha_5 = 0$ for the $qqqq\nu\nu$ final state arising from a fit to $\cos\theta_{\text{jets}}^*$ at 1.4 TeV for different values of jet reconstruction parameters. | 32 |
| A.3. χ^2 as a function of α_5 assuming $\alpha_4 = 0$ for the $qqqq\nu\nu$ final state arising from a fit to $\cos\theta_{\text{jets}}^*$ at 1.4 TeV for different values of jet reconstruction parameters. | 33 |

List of tables

| | |
|---|----|
| 1.1. Cross section for selected processes for given value of α_4 and α_5 at 1.4 TeV. | 5 |
| 1.2. Cross section for selected processes for given value of α_4 and α_5 at 3 TeV. | 5 |
| 1.3. 1σ precision on measurement of α_4 for different jet reconstruction parameters considering pure signal at 1.4 TeV. | 16 |
| 1.4. 1σ precision on measurement of α_5 for different jet reconstruction parameters considering pure signal at 1.4 TeV. | 16 |
| 1.5. 1σ precision on measurement of α_4 for different jet reconstruction parameters considering pure signal at 3 TeV. | 17 |
| 1.6. 1σ precision on measurement of α_5 for different jet reconstruction parameters considering pure signal at 3 TeV. | 17 |
| 1.8. Number of events passing the various cuts applied in the preselection at 1.4TeV. | 22 |
| 1.9. Number of events passing the MVA selection at 1.4TeV. | 26 |